Acta Crystallographica Section D
Biological Crystallography
ISSN 0907-4449

Structure of the C-terminally truncated human ProMMP9, a gelatin-binding matrix metalloproteinase

Patricia A. Elkins,[a]* Yen Sen Ho,[a] Ward W. Smith,[a] Cheryl A. Janson,[a] Karla J. D'Alessio,[a] Michael S. McQueney,[a] Maxwell D. Cummings[b] and Anne M. Romanic[a]

[a]GlaxoSmithKline, King of Prussia, Pennsylvania 19406, USA, and [b]3-Dimensional Pharmaceuticals, Exton, Pennsylvania 19341, USA

Correspondence e-mail: patricia_a_elkins@gsk.com

Received 1 March 2002
Accepted 29 April 2002

PDB Reference: human ProMMP9, 1l6j, r1l6jsf.

The X-ray crystal structure of the proform of human matrix metalloproteinase MMP9 has been solved to 2.5 Å resolution. The construct includes the prodomain, the catalytic domain and three FnII (fibronectin type II) domains. The prodomain is inserted into the active-site cleft, blocking access to the catalytic zinc. Comparison with the crystal structure of the most closely related MMP, MMP2, indicates that the conformations of residues in the active-site cleft and in the cysteine-switch peptide of the prodomain are highly conserved and that design of MMP9-specific inhibitors will be challenging. In common with MMP2, the MMP9 S1′ inhibitor-binding pocket is large compared with that of other MMPs. One small point of difference in the S1′ binding pockets of MMP9 and MMP2 may provide an opportunity to explore the design of specific inhibitors. The side chain of Arg424 in MMP9 is angled slightly away from the S1′ pocket when compared with the corresponding residue in MMP2, Thr424. The secondary structure of the FnII domains is conserved between the two closely related MMPs, although the second FnII domain makes no contact with the catalytic domain in MMP9, while the same domain in MMP2 has a substantial area of interaction with the catalytic domain.

1. Introduction

Matrix metalloproteinases (MMPs) are a family of structurally and functionally related zinc-containing enzymes that degrade the extracellular matrix of the basement membrane (Woessner, 1991). Physiologically, MMPs are involved in normal processes of wound healing, bone resorption and mammary involution (McCawley & Matrisian, 2001). However, MMPs also play a fundamental role in a wide variety of pathological conditions including rheumatoid arthritis (Shaw *et al.*, 2000), cardiovascular diseases (Spinale *et al.*, 2000; George, 2000) and cancer (John & Tuszynski, 2001; Kugler, 1999). MMPs contribute to joint destruction in rheumatoid arthritis by degrading the cartilage and bone (Jackson *et al.*, 2001). The activity of MMPs is not only essential for the formation of atherosclerotic plaque, but is also important in its degradation. Dissolution of plaque may cause plaque instability and rupture, eventually leading to the clinical symptoms of atherosclerosis, unstable angina, myocardial infarction and stroke (George, 2000). Many studies have shown that MMPs play important roles in tumor invasion, metastasis and angiogenesis in various cancer types including lung cancer, colon cancer, breast cancer (Yao *et al.*, 2001), bladder cancer (Kanayama, 2001) and prostate cancer (Lokeshwar, 1999). Thus, inhibition of the enzyme action of MMPs provides a particularly attractive target for therapeutic intervention in these life-threatening diseases.

In recent years, numerous studies have shown the importance of MMP9 in cancer and atherosclerosis. For example, in colorectal, breast, prostate and bladder cancer, most patients with aggressive disease have increased plasma levels of MMP9 (Zucker *et al.*, 1999). In advanced colorectal cancer, high levels of MMP9 have been associated with shortened survival (Yao *et al.*, 2001). In cardiovascular diseases, MMP9 has been identified in human atherosclerotic lesions and the enhanced expression of MMP9 has been linked to plaque rupture (Galis *et al.*, 1995; Spinale *et al.*, 2000).

MMPs are divided into the following subgroups according to substrate specificities. The most widely studied of these are the collagenases (MMP1, MMP8, MMP13), gelatinases (MMP2, MMP9), stromelysins (MMP3, MMP10), a mixed subgroup which includes matrilysin (MMP7) and the membrane-bound MMPs (MT-MMPs, MMP-11). All MMPs are produced as proenzymes. Comprehensive sequence alignments (Massova *et al.*, 1998) confirm the generally conserved domain structure of a propeptide of approximately 80 amino acids, a catalytic domain of about 165 residues, a short linker region and a matrix-binding domain of almost 200 amino acids referred to as the hemopexin-like domain. Proteolytic cleavage of the propeptide is required for activation of the enzyme. MMP catalytic domains are characterized by high sequence and structural homology. These domains are α/β-domains with conserved binding sites for structural and catalytic Zn atoms and for two or three Ca atoms.

The DNA sequence of MMP9, human 92 kDa type IV collagenase/gelatinase, was first reported by G. I. Goldberg (Wilhelm *et al.*, 1989). The preproenzyme contains 707 amino-acid residues, including a 19 amino-acid signal peptide. The human MMP9 proenzyme consists of five domains. The amino-terminal propeptide, the zinc-binding catalytic domain and the carboxyl-terminal hemopexin-like domain are conserved throughout the MMP family. The fibronectin-like domain cluster is also found in MMP2, while the proline-rich collagen-like domain is unique to MMP9 (Collier *et al.*, 1988). MMP9 and the closely related 72 kDa MMP2 degrade type IV collagen and denatured collagen or gelatin. Both MMP9 and MMP2 contain three FnII motifs which are thought to mediate gelatin binding (Murphy *et al.*, 1994). Recombinant MMP FnII domains have been shown to have significant gelatin-binding activity (Collier *et al.*, 1992; Banyai & Patthy, 1991; Banyai *et al.*, 1994) and gelatinases expressed without FnII domains lack gelatin-binding activity (Murphy *et al.*, 1994; Allan *et al.*, 1995). The sequences for the small FnII domains are inserted into the sequence of the catalytic domain, but the FnII domains fold as separate units adjacent to the catalytic domain. The insertion of the FnII domains in MMP9 does not perturb the structure of the catalytic domain.

Clinical trials of compounds with efficacy as cancer treatments in the USA, Europe and Canada have involved several synthetic low-molecular-weight inhibitors of MMP activity, including batimastat (BB-94), marimastat (BB-2516) and bryostatin among others. Coussens *et al.* (2002) and Wojtowicz-Praga *et al.* (1997) review the clinical trials and give structures of these compounds. Preclinical studies showed that treatment of heart failure in animal models with MMP inhibitors results in less tissue damage and improved cardiac function (Li & Feldman, 2001). Limited clinical trials have been undertaken for rheumatoid arthritis (Jackson *et al.*, 2001; Shaw *et al.*, 2000; Elliott & Cawston, 2001). The results are equivocal, but inhibition of MMPs remains a primary therapeutic target in rheumatoid arthritis.

Structural studies of MMPs have elucidated molecular details of many of the MMP family members. A comprehensive review of common MMP structural features can be found in Bode *et al.* (1999). To date, more than 50 crystal structures of MMPs have been published. These include full-length proMMPs, activated MMPs, catalytic domains alone and inhibitor-bound MMPs. The X-ray crystal structure of proMMP2 (Morgunova *et al.*, 1999) includes the entire proMMP2 and demonstrates the conservation of the structure of the gelatinase catalytic domain with those of other MMPs.

Protease inhibitors that can selectively bind to MMP9 are expected to be of value in treating a variety of pervasive and costly diseases. An understanding of the overall tertiary structure of MMP9 in general, and the catalytic domain in particular, will provide important information for the structure-directed design of new enzyme inhibitors. Therefore, a MMP9 construct was prepared that includes the propeptide, the catalytic domain and the three FnII domains and the crystal structure of this proMMP9 construct was determined. This is the first crystal structure of MMP9 to be published. The structure is quite similar to the structure of proMMP2 with the exception of the placement of the FnII domains. Conservation of the residues that line the active site and conservation of the conformation of the side chains of those residues is high; however, the shape and size of the MMP9 S1′ inhibitor-binding pocket may provide an avenue for designing MMP9- or gelatinase-specific inhibitors.

2. Materials and methods

2.1. Cloning and expression

Two gene-specific primers of human MMP9 (Genbank accession No. J05070) were synthesized. Primer 1 (5′-GCAATTACTGATACCATGGCCCCCAGACAGCGCCAGTCCACCCTTG-3′) incorporates sequences for a unique *Nco*I site and an initiating methionine. Primer 2 (5′-GCGACGGCATCACTCGAGGTCGACTCAACCATAGAGGTGCCGGATGCCATTCACGTCGTCC-3′) incorporates sequences for a stop codon and a unique *Sal*I site. Using these two primers, a 1275 bp DNA fragment was obtained from both human lung and spleen cDNA libraries (SuperScript cDNA libraries, Life Technologies, Rockville, MD, USA) by polymerase chain reaction (PCR). These fragments were digested with *Nco*I and *Sal*I and ligated into the *Nco*I and *Sal*I sites of the T7 expression vector of pET-28a-c(+) (Novagen Madison, WI, USA). Two recombinant plasmids were constructed and confirmed by sequencing. They were termed PC-MMP9 clones 7 and 8, which were derived from human lung and spleen cDNA libraries, respectively. Mole-

cular cloning in this study was performed according to standard procedures (Sambrook *et al.*, 1989).

For expression in *Escherichia coli*, PC-MMP9 clones 7 and 8 were transformed into BLR (DE3) (according to the manufacturer's manual). For induction, a single colony was picked from a freshly streaked plate, inoculated into 10 ml LB containing 50 μg ml^{-1} kanamycin and incubated overnight with shaking at 310 K. 0.25 ml of the overnight culture was then inoculated into 50 ml fresh medium plus antibiotic and incubated with shaking at 310 K until OD_{600} reached 0.6–0.7. Samples were removed for the uninduced control. To the remainder, IPTG from a 100 m*M* stock was added to a final concentration of 0.4 m*M*. During incubation, aliquots were taken at 3, 4 and 5 h following IPTG induction. Samples were placed on ice for 5 min and the cells were then harvested by centrifugation at 5000*g* for 5 min at 277 K. The supernatant was removed and the cell pellet was used for SDS–PAGE and Western blot analysis. The remainder of the cells were stored at 203 K for further analysis.

For Western blot analysis, cell pellets were boiled in reducing SDS sample buffer, analyzed by SDS–PAGE and transferred onto a nitrocellulose membrane. The membrane was then blocked with 5% non-fat milk in PBS and probed with polyclonal anti-MMP9 antibody (mouse anti-human MMP-9 Ab, Clone #7-11C; Oncogene Research Products, Cambridge, MA, USA), followed by the appropriate HRP-conjugated secondary antibody. Finally, the protein bands were visualized by chemiluminescence using an ECL Western blotting detection kit (Amersham Corp.).

2.2. Activity analysis

MMP9 enzyme activity was assayed by SDS–PAGE zymography using gelatin as a substrate. The proMMP9 sample was subjected to electrophoresis, without boiling or reduction, through a 10% polyacrylamide gel co-polymerized with 0.5 mg ml^{-1} gelatin (Novex, San Diego, CA, USA) at 277 K. After electrophoresis was completed, the gel was incubated for 1 h at 298 K in a 2.5% Triton X-100 solution, washed two times (20 min each) with water and then incubated overnight at 310 K in 0.05 *M* Tris–HCl buffer pH 8.0 containing 5 m*M* $CaCl_2$. The gel was fixed with 40% methanol and 7% acetic acid, stained with 0.25% Coomassie brilliant blue R250 and then destained with 10% methanol and 7% acetic acid. Enzyme activity attributed to proMMP9 was visualized in the zymogram as a clear band against a dark background.

2.3. Purification

The *E. coli* cell pellet (31 g wet weight) was suspended into 250 ml of 25 m*M* Na_2HPO_4, 150 m*M* NaCl pH 7 (PBS) using a Tekmar tissuemizer and processed twice through a cell disrupter (Avestin, Inc.) at 69 MPa. After centrifugation at 16 000*g* for 90 min, the lysate pellet was suspended using the tissuemizer into 250 ml of PBS containing 10 m*M* DTT, 1 m*M* EDTA and processed through the cell disrupter once. Following centrifugation at 26 000*g* for 30 min, the washed lysate pellet was solubilized using the tissuemizer into 200 ml of freshly prepared 8 *M* urea, 25 m*M* Tris, 10 m*M* DTT, 1 m*M* EDTA pH 7.5. The suspension was stirred overnight at room temperature on a stir plate at medium speed, then centrifuged at 26 000*g* for 30 min. The supernatant containing solubilized denatured proMMP9 was clarified by filtration using an AP15 prefilter and a 1.2 μm PVDF low-protein-binding membrane (Millipore). The filtrate was assayed for protein concentration according to the method of Bradford using the Bio-Rad protein-assay reagent and bovine serum albumin (Pierce) as a standard reference. The denatured protein solution (200 ml, 3.4 mg ml^{-1}) was applied at a linear flow rate of 34 cm h^{-1} (3 ml min^{-1}) onto a 2.6 × 11 cm column of Source Q anion-exchange resin (Pharmacia) pre-equilibrated in 8 *M* urea, 25 m*M* Tris pH 7.5 (buffer *A*). Following a wash to baseline OD with buffer *A*, bound proMMP9 was eluted at a linear flow rate of 45 cm h^{-1} (4 ml min^{-1}) using a 10 column volume gradient (580 ml) of buffer *A* containing 0.25 *M* NaCl pH 7.5. Column fractions (8 ml) containing proMMP9 were pooled based upon purity as judged on a 4–20% acrylamide Tris–glycine SDS–PAGE gel (Novex). The pooled proMMP9 protein (115 ml, 2.8 mg ml^{-1}) was slowly added dropwise to a stirred room-temperature 10 l solution of 20 m*M* Tris, 200 m*M* NaCl, 5 m*M* $CaCl_2$, 1 m*M* $ZnCl_2$, 0.7 *M* L-arginine, 10 m*M* reduced and 1 m*M* oxidized glutathione pH 7.5 to yield a 32 μg ml^{-1} protein solution. After stirring overnight at 277 K, the solution was concentrated to 4 l using a tangential flow unit fitted with an Omega 10K membrane (Pall Filtron). 1,10-Phenanthroline was then added to 5 m*M* and the solution was further concentrated to 150 ml using a stirred cell fitted with a YM-10 membrane (Amicon). Following clarification using a 0.45 μm PVDF membrane (Millipore), the solution was dialyzed overnight at 277 K against 5 l of 20 m*M* Tris, 100 m*M* NaCl, 5 m*M* 1,10-phenanthroline pH 7.5. The 150 ml dialysate was again clarified by centrifugation (26 000*g*, 30 min) and 0.45 μm filtration and then further concentrated to 50 ml using a stirred cell. The clarified concentrate (50 ml, 1.6 mg ml^{-1}) was applied at a linear flow rate of 22.6 cm h^{-1} (2 ml min^{-1}) in two batches to a 2.6 × 99 cm column of Superdex 75 pre-equilibrated in 20 m*M* Tris, 100 m*M* NaCl pH 7.5. 80 mg of pure monomeric pMMP9 was pooled based upon purity as judged by SDS–PAGE. The protein was further concentrated to 12.8 mg ml^{-1} using an Amicon stirred cell.

2.4. Crystallization

Crystals were grown by vapor diffusion in sitting drops. Drops were prepared by mixing equal amounts of the protein solution at 12.8 mg ml^{-1} in 20 m*M* Tris pH 8.2, 100 m*M* NaCl with mother liquor consisting of 4.3 *M* NaCl, 0.1 *M* HEPES pH 7.0 and placed over a reservoir of mother liquor at 293 K. Crystals grew in 3 d to dimensions of 0.1 × 0.1 × 0.25 mm. Crystals grew as hexagons in space group $P6_5$, with unit-cell parameters $a = b = 123.7$, $c = 89.9$ Å, and diffracted to 2.5 Å with synchrotron radiation. There is one molecule per asymmetric unit and the unit cell has a solvent content of 70.7%.

2.5. Data collection

Crystals were flash-cooled by submersion in liquid nitrogen without additional cryoprotectant. A potential derivative was prepared by soaking a crystal in 5 m*M* K_2IrCl_6 for 3 d. Data were collected from the derivative crystal at the National Synchrotron Light Source, Brookhaven National Laboratory at wavelengths near the peak of the zinc absorption spectra measured for the crystal. 110° of data at three wavelengths were collected for a MAD experiment (Table 1). Data were processed using the *DENZO*/*HKL* (Otwinowski & Minor, 1997) software packages.

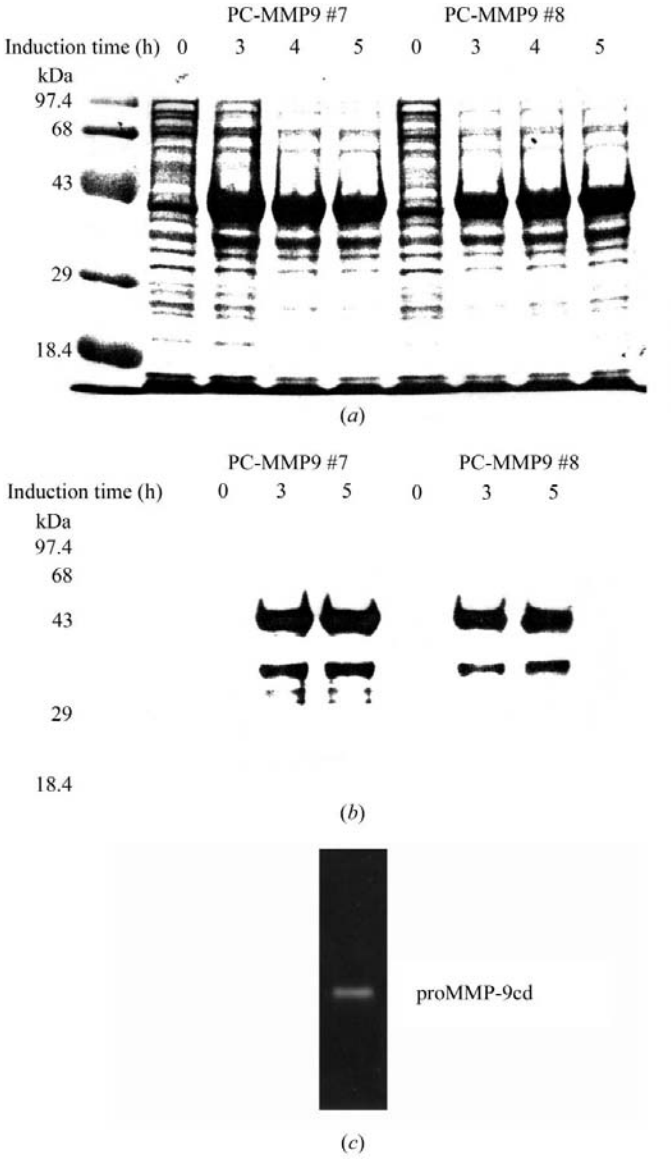

Figure 1
Induced expression of proMMP9 in *E. coli*. *E. coli* cells transformed with PC-MMP9 clone 7 and clone 8 were incubated at 310 K until the OD_{600} reached 0.6–0.7 and were then induced by IPTG at a final concentration of 0.4 m*M*. Samples were taken at 0, 3, 4 and 5 h following induction. The cell pellets, collected from 100 µl of cell culture, were resolved on 15% SDS–PAGE gels and processed with Coomassie brilliant blue staining (*a*; samples taken at 0, 3, 4 and 5 h) and Western blotting with anti-MMP9 Ab (*b*; samples taken at 0, 3 and 5 h). (*c*) The expressed proMMP9 protein, proMMP9-cd, was analyzed for enzyme activity by SDS–PAGE gelatin zymography. Gelatinolytic activity, visualized as a clear band against a dark background, was observed at a molecular weight of approximately 47 kDa.

Table 1
Data collection and refinement statistics.

Values in parentheses are for the highest resolution shell.

	Peak	Inflection	Remote
Data collection			
Resolution (Å)	2.5 (2.59–2.50)	2.5 (2.59–2.50)	2.5 (2.59–2.50)
Wavelength (Å)	1.271632	1.209997	1.272917
Total reflections	47453 (3904)	47462 (3930)	46373 (3804)
Completeness (%)	89.1 (73.8)	88.7 (73.2)	86.1 (70.3)
$I/\sigma(I)$	11.5 (2.4)	10.1 (2.0)	10.5 (2.4)
R_{merge} (%)	7.7 (19.4)	7.5 (21.8)	6.8 (17.5)
Refinement statistics			
Resolution (Å)	20.0–2.5 (2.53–2.50)		
Total reflections	24477 (783)		
Reflections for R_{free}	1265 (39)		
R_{cryst}/R_{free}	18.0/22.3		
R.m.s. deviations			
Bonds (Å)	0.012		
Angles (°)	1.7		
Water molecules	230		
Average *B* factors (Å^2)			
Protein	37		
Solvent	37		
R.m.s. deviations in *B* factors			
Main-chain bonds (Å^2)	2.1		
Main-chain angles (Å^2)	3.5		
Ramachandran plot (% residues)			
Most favored regions	83.5		
Additionally allowed regions	15.6		
Generously allowed regions	0.9		
Disallowed regions	0.0		

2.6. Structure solution

The positions of the Zn atoms were identified using the software package *SOLVE* (Terwilliger & Berendzen, 1999) using all data to 2.5 Å and ignoring any contribution Ir atoms might make to scattering at the wavelengths used for the MAD data collection. The *SOLVE* solution was unambiguous, with a *Z* score of 49 and a mean figure of merit of 0.33. Owing to the high solvent content of the crystals, solvent flattening as implemented in the program *DM* (Cowtan, 1994) resulted in a substantial improvement in map quality. *SOLVE* and *DM* were run in space groups $P6_5$ and $P6_1$ to determine the correct space group of the crystal.

2.7. Model building and refinement

Data measured at the shortest wavelength, $\lambda = 1.209997$ Å, were used for the refinement. Electron density for the three histidines that coordinate each of the zinc ions was excellent and was immediately obvious by visual inspection of the *DM* electron-density map calculated in space group $P6_5$. Using the graphics-display program *O* (Jones *et al.*, 1991), the X-ray crystal structure of MMP2 was rotated and translated manually into the electron density until the histidines coordinating

the Zn atoms fit into the electron density for those side chains. Most domains of the MMP2 model fit well into the electron density, with the exception of the second FnII domain. The electron density was considerably less well defined for this domain, but was sufficient to indicate the general orientation and placement of the domain. The model was refined using *CNS* (Brünger *et al.*, 1998). The structure was validated with the program *PROCHECK* (Laskowski *et al.*, 1993).

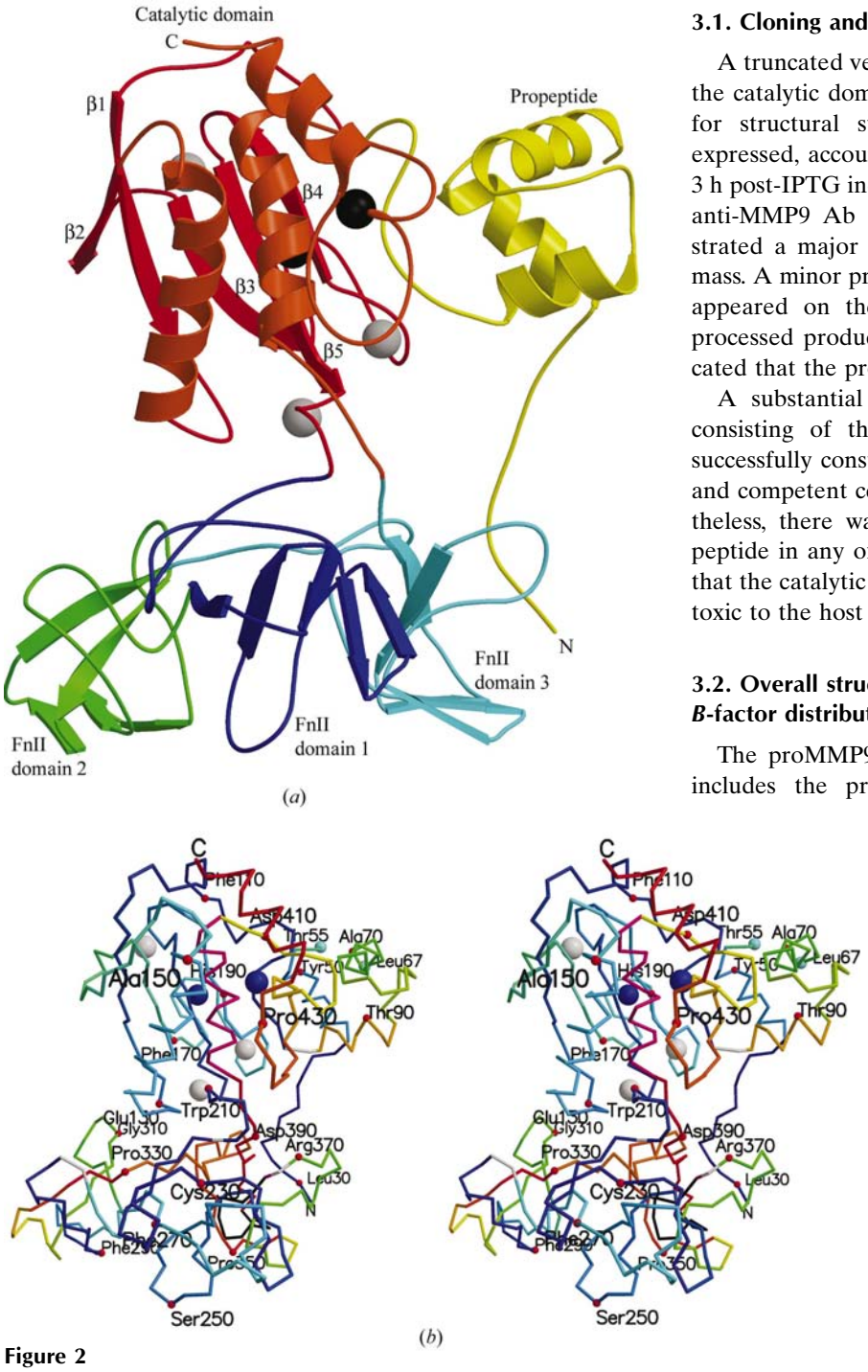

Figure 2
(*a*) Ribbon drawing of proMMP9. The propeptide is in yellow, the catalytic domain is shown in red (strands) and orange (helices) and the three FnII domains are in blue, green and cyan. Ca atoms are shown as grey spheres and Zn atoms as black spheres. All structure figures were prepared using the programs *MOLSCRIPT* (Kraulis, 1991) or *BOBSCRIPT* (Esnouf, 1997) and the *Raster3D* molecular-graphics package (Bacon & Anderson, 1988; Merritt & Murphy, 1994). (*b*) C^{α} trace of the proMMP9 structure. Every 20th residue is marked by a small red ball and the endpoints of the missing stretch of residues, Thr55 and Leu67, are marked with a blue ball. The chain is colored to make it possible to follow the chain trace.

3. Results and discussion

3.1. Cloning and expression

A truncated version of MMP9 consisting of the propeptide, the catalytic domain and the three FnII domains was cloned for structural studies. The MMP9 construct was highly expressed, accounting for 60% of the total *E. coli* protein in 3 h post-IPTG induction (Fig. 1*a*). Western blot analysis using anti-MMP9 Ab (Fig. 1*b*) and SDS–PAGE analysis demonstrated a major protein band with the predicted molecular mass. A minor protein band with a lower molecular mass also appeared on the Western blot, which might represent a processed product of MMP9. SDS–PAGE zymography indicated that the proMMP9 construct is active (Fig. 1*c*).

A substantial effort was made to produce a construct consisting of the catalytic domain alone. The gene was successfully constructed. Several different expression vectors and competent cell lines were tried for its expression. Nevertheless, there was no detectable expression of the desired peptide in any of the experiments, leading to the conclusion that the catalytic domain of MMP9, in its active form, may be toxic to the host cell.

3.2. Overall structure description and quality of model, *B*-factor distribution

The proMMP9 construct consists of residues 20–444 and includes the propeptide (residues 20–109), the catalytic domain (residues 110–215 and 390–444) and the three FnII domains (residues 216–389), but does not include the MMP9 collagen-like domain or the large C-terminal hemopexin-like domain. The structure is illustrated in Fig. 2. The three FnII domains cluster at the tip of the elongated catalytic domain, with the small propeptide associated with one side of the catalytic domain. The extended N-terminus of the protein reaches from an interaction with one of the three FnII domains up to the active-site cleft of the catalytic domain where the three helices of the prodomain are clustered. The overall average temperature factor for both the protein and the 230 water molecules is 37 Å^2. Within the protein, the average temperature factors vary by domain from 29 Å^2 for the catalytic domain and 37 Å^2 for the propeptide to 47 Å^2 for the three FnII domains. The Ramachandran plot indicates that 83.5% of the residues fall into the most favored regions, 15.6% of the residues are in the

additional allowed region and three residues are in the generously allowed region. The final R_{cryst} for the structure was 18.0% and the final R_{free} was 22.3%. Statistics for the refinement are reported in Table 1. Electron density for the solvent-flattened MAD-phased initial map was excellent. Fig. 3 illustrates the density for the histidine and cysteine side chains around the catalytic zinc in the initial map.

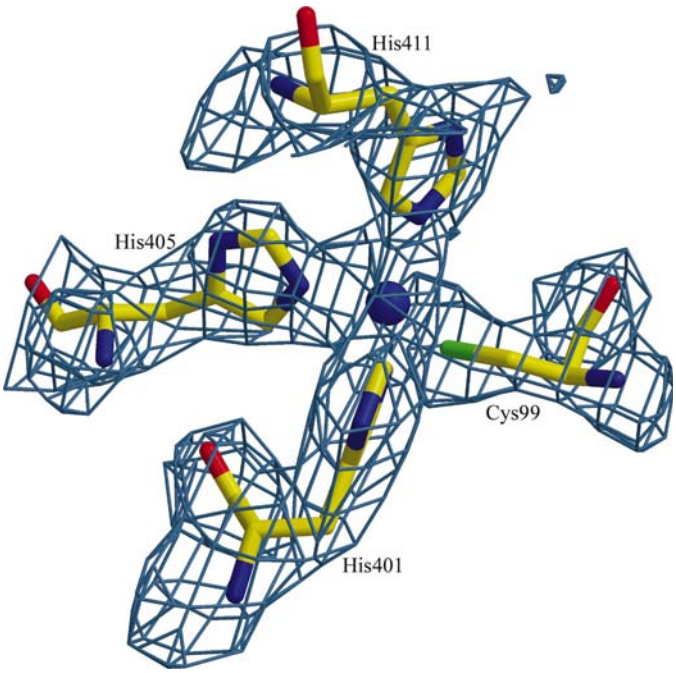

Figure 3
Electron density calculated for the solvent-flattened MAD-phased initial map. Density covers His401, His405, His411 and Cys99, the side-chain ligands to the conserved catalytic zinc. The Zn atom is represented as a blue sphere.

3.3. Structure of the propeptide

The propeptide folds into a small domain that is closely associated with the catalytic domain. MMP9 is activated by autoproteolytic cleavage of the propeptide *in vivo* or *in vitro* by reacting with an organomercurial compound or other proteases such as trypsin or chymotrypsin (Triebel *et al.*, 1992; Okada *et al.*, 1992; Morodomi *et al.*, 1992). Disruption of the intimate interaction of the prodomain with the catalytic domain occurs when the propeptide is cleaved from the catalytic domain on activation. The secondary structure of the propeptide consists of a cluster of three α-helices that lie roughly perpendicular to each other. The N-terminal nine residues of the construct are disordered, as is the loop connecting the first two helices; these residues are not included in the model. The stretch of amino acids between the first ordered residue of the construct, Val29, and the first residue of the first helix, Thr40, bridges a gap between the third FnII domain and the compact remainder of the globular propeptide domain. On the N-terminal side of this gap, the side chain of Phe31 is tucked against the hydrophobic side chains of residues Trp372, Phe379 and Trp385 of the third FnII domain as shown in Fig. 4. The backbone carbonyl group of Pro32 makes a hydrogen bond with the side chain of Trp385 (2.9 Å). Fig. 5 illustrates the stretch of propeptide residues 97–99 that is inserted in the active-site groove between two relatively parallel stretches of amino acids (residues Gly186–Ala191 at the N-terminus of strand β4 and residues Pro421–Tyr423). Main-chain–main-chain hydrogen bonds are formed between the three short stretches of amino acids, effectively extending the β-sheet of the catalytic domain (Fig. 5). The position of Cys99 within the active site to coordinate the active-site Zn^{2+} ion results in the active-site cleft being sequestered from solvent by the prodomain. Cleavage of the propeptide opens up the active site, facilitating interactions with substrate or inhibitors.

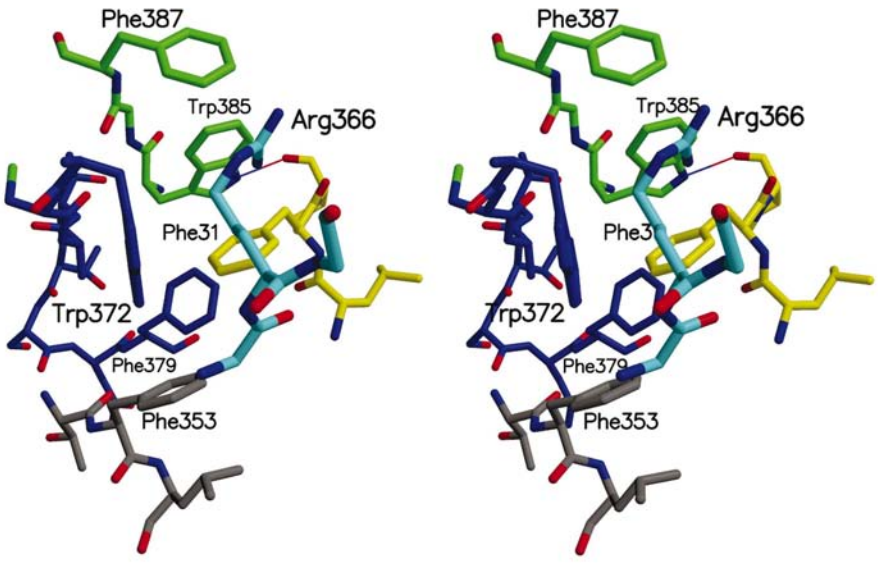

Figure 4
Stereoview of Phe31 of the propeptide that interacts with a cluster of aromatic side chains in the third FnII domain.

3.4. Structure of the catalytic domain

The catalytic domain of MMP9 is an example of a matrixin fold (Stocker & Bode, 1995) and is a slightly elongated globular domain with a diameter of approximately 40 Å. The domain consists of five β-strands in a twisted β-sheet layered against three helices. Metal ions are closely associated with the β-sheet, with one Zn atom above and one Zn atom below the plane of the sheet; Ca atoms are located at the ends of the sheet. Residues between the two layers are hydrophobic and for the most part aromatic. A number of the structural features observed in the MMP9 catalytic domain are conserved among MMPs (Fig. 6) (Bode *et al.*, 1999). Among these are (i) a loop between strands β3 and β4 which forms an

'S-shaped double loop' that clamps both the structural Zn^{2+} ion and one Ca^{2+} ion in place near the end of the active-site cleft, (ii) the 'bulge-edge' of the active-site cleft which includes residues N-terminal to and part of strand β4 and is involved in binding of inhibitors and peptide substrates, (iii) a conserved sequence motif HE*xx*H*xx*G*xx*H, characteristic of the metzincin zinc-endopeptidase superfamily (Bode *et al.*, 1993; Stocker *et al.*, 1995) and partly displayed on helix αB, (iv) conserved residues Pro421–*X*–Tyr423 which form the wall of the inhibitor-binding S1′ pocket and (v) the specificity loop curling behind the S1′ pocket, residues Arg424–Pro430.

3.4.1. Metal-binding sites. Two Zn^{2+} ions, a catalytically important zinc and a zinc that plays a structural role, are conserved among MMP structures. The catalytic Zn^{2+} is located in the active site of the enzyme and is coordinated tetrahedrally by three histidine side chains (2.1 Å bond distance in each case), His401, His405 and His411, which are part of the conserved consensus sequence HE*xx*H*xx*G*xx*H that curves around one end of the active-site cleft. The fourth ligand is the side chain of Cys99, the single cysteine residue in the propeptide. From one side of the active-site cleft, the side chains of His401 and His405 stick into the cleft from adjacent turns of helix αB. From the C-terminal end of helix αB, the protein rounds the end of the cleft and makes a sharp turn back towards the catalytic zinc, positioning His411 as a third ligand.

The structural Zn^{2+} also has three histidine side-chain ligands. His175 (2.2 Å) is on the loop between strands β3 and β4, and His190 (2.2 Å) and His203 (2.1 Å) are on neighbouring β-strands β4 and β5. The fourth ligand is the conserved Asp177 (2.2 Å). This zinc is sandwiched between the outer face of strand β5 and the S-shaped double loop that connects strands β3 and β4 and wraps back over strand β5. The orientation of these histidine residues relative to the two zinc ions is identical to that found in the proMMP2 structure.

Three Ca^{2+} ions are found in conserved positions in many structures of MMPs, including MMP9. Each of the three Ca^{2+} ions has an octahedral coordination. One Ca^{2+} ion is located within the C-terminal portion of the S-shaped double loop that wraps around the Ca^{2+} ion. This calcium is ligated by side-chain and backbone residues of Asp182 (2.7 Å), Gly183 (2.4 Å), Asp185 (2.4 Å) and Leu187 (2.6 Å) and, in strand β5, residues Asp205 (2.4 Å) and Glu208 (2.5 Å). All but Asp185 are highly conserved residues among MMPs. A second Ca^{2+} atom is located near the first Ca^{2+}, at the edge of the β-sheet, coordinated by Asp131 (2.8 Å), Asp206 (2.5 Å), Asp206 (2.8 Å) and Glu208 (2.6 Å) and by two water molecules. The third Ca^{2+} ion is primarily coordinated by residues in the loop between β4 and β5, residues Gly197 (2.9 Å), Gln199 (2.5 Å)

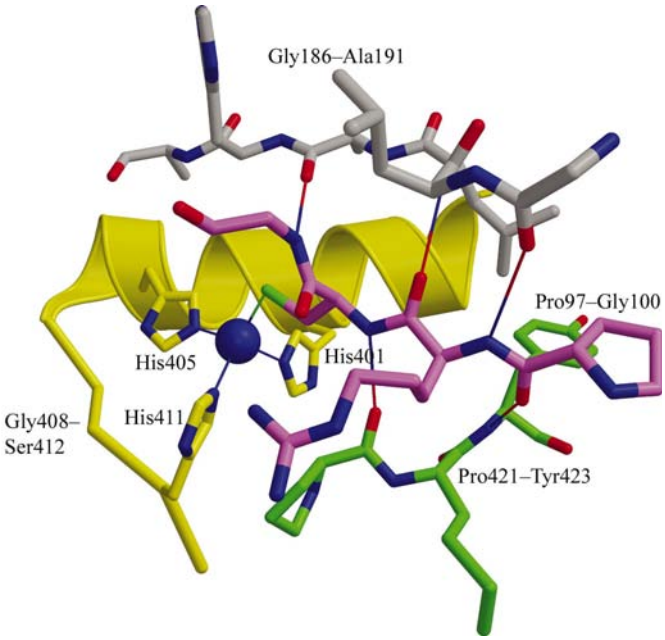

Figure 5
Ball-and-stick drawing of the active-site cleft. The cleft is delineated by the bulge-edge strand, residues 186–191, shown in grey, which runs horizontally across the figure. Helix αB in yellow runs along the bottom of the cleft. In green are shown residues 421–423 of the S1′ pocket wall-forming segment and in magenta are residues 97–100, including Cys99 of the switch peptide. Side chains for His401, His405 and His411 of the conserved histidine sequence motif are shown with dashed lines indicating bonds to the catalytic zinc, represented as a blue sphere. Hydrogen bonds are indicated between backbone atoms of the bulge-edge strand, the prodomain cysteine-switch peptide and the wall-forming segment. The switch peptide fits into the deep part of the cleft. The shallow end of the active-site cleft is bounded by residues 409–410.

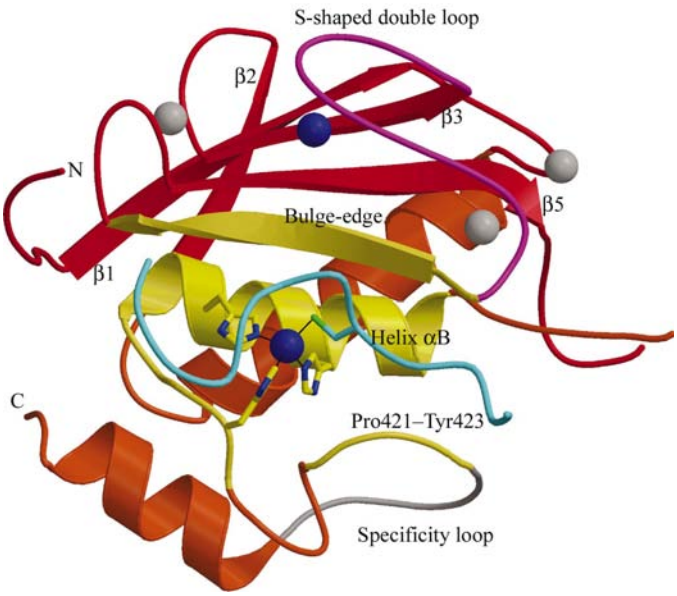

Figure 6
Ribbon close-up of the catalytic domain. The S-shaped double loop is shown in magenta in the upper right portion of the figure. Elements forming the active-site cleft are shown in yellow. These include the bulge-edge strand (β4) of the active-site cleft, helix αB that lines the bottom of the cleft and the segment that forms the wall of the S1′ pocket, residues Pro421–Tyr423, which is shown as a yellow coil in the lower right portion of the figure. Histidine side chains from the conserved sequence motif are indicated surrounding the catalytic zinc. Side chains of the specificity loop, indicated in the lower part of the figure as a light grey coil, wrap under the S1′ binding pocket. Residues 97–100 of the propeptide are depicted as a cyan-colored coil and the side chain of Cys99 is shown in cyan as a ligand to the active-site zinc. The Zn atoms are shown in blue and the Ca atoms are shown in grey.

and Asp201 (2.5 Å), as well as Asp165 (2.6 Å) and two water molecules.

3.4.2. Active site. An important feature of the catalytic domain is the active-site cleft. In structures of MMPs, the active-site cleft can be filled with the propeptide, peptide substrates or inhibitors. The structure of the active site can be described according to the convention for proteases with respect to the sites on the enzyme, labelled S2, S1, S1′ and S2′, that bind corresponding portions of inhibitors specified as P2, P1, P1′ and P2′ (Schechter & Berger, 1967). Designations indicate both proximity to the scissile bond, with lower numbers closer to the bond, and location with respect to the substrate, the unprimed sites being towards the N-terminus of the substrate and the primed sites being near the C-terminal side of the substrate (Stocker *et al.*, 1995). In the proenzyme structure, access to the active-site cleft is blocked by the cysteine-switch peptide (Van Wart & Birkedal-Hansen, 1990), a stretch of residues in the proenzyme centered around Cys99 coordinating the active-site Zn^{2+} (Fig. 5). Relatively parallel to each other and delineating the active-site cleft are the bulge-edge strand β4 (residues 186–191) along one side, the segment that forms the wall of the S1′ pocket (residues 421–423) along the other side (antiparallel in direction to strand β4) and helix αB which forms the floor of the cleft. The propeptide (residues 97–101) runs through the active-site cleft parallel to strand β4. It fills the solvent-accessible portion of the cleft but leaves the S1′ pocket empty except for a network of water molecules. The chemistry of cleavage of the scissile P1–P1′ substrate peptide bond involves activation of a catalytic water by the catalytic Glu402 located close to the active-site zinc. Both the bulge-edge strand β4 and the wall-forming segment make extensive main-chain–main-chain hydrogen-bonding interactions with the propeptide strand within the active-site cleft. The size of the S1′ binding pocket varies among MMPs and is determined by the conformation of large side-chain residues that line the pocket. The proMMP9 S1′ pocket is large for an MMP as there are no sizeable side-chain residues occluding the active-site cleft. The MMP9 S1′ pocket is primarily lined with main-chain carbonyl O atoms of residues Pro415–Leu418 and Tyr420–Tyr423 and the side chains of Leu397 and Thr426. In contrast, the shape and size of the S2′ pocket is conserved among MMPs. This binding site is primarily shaped by residues Gly186–Leu188, a small loop at the N-terminal end of strand β4. On the other side of the catalytic zinc, the S1 site generally interacts with an extension of the zinc-binding group (Chen *et al.*, 1999) and is in the relatively flat shallow end of the active-site cleft. Conservation of the backbone conformation for residues that define the S1 site is high, although side chains vary among the MMPs. Analogous residues in MMP9 to those identified as part of the S1 site in MMP3 (Chen *et al.*, 1999) are Tyr179, His190, Asp410 and His411.

3.5. Structure of the FnII domains

The three FnII domains cluster in an approximate trefoil arrangement at one end of the catalytic domain. The three domains have almost identical conformations, with a least-squares r.m.s. deviation of 0.7 Å or less for 50 C^{α} atoms per domain. These domains have characteristic sequence motifs, which include four disulfide-bonded cysteines and four aromatic residues. The proMMP9 structure has the canonical FnII domain structure consisting of two double-stranded antiparallel β-sheets that are oriented approximately at right angles to each other, with conserved aromatic residues clustered between the β-sheets (Pickford *et al.*, 1997). However, a slight perturbation in the conformation of one connecting loop, residues 260–262 in the first FnII domain, results in a third parallel strand interaction in the second β-sheet in each FnII domain.

In the FnII domains, a cluster of aromatic residues forms a shallow hydrophobic surface. For the third MMP9 FnII domain, these residues are illustrated in Fig. 4. This cluster consists of Phe353, Trp372, Phe379, Trp385 and Phe387 and the pocket they form with the alkyl side chain of a highly conserved arginine residue Arg366 is filled by Phe31 from the N-terminus of the propeptide. The homologous hydrophobic surfaces in the other two FnII domains are each capped by two water molecules that bridge between the conserved arginine and one of the phenylalanine residues in the aromatic cluster. Alanine-scanning mutagenesis of the second MMP9 FnII domain has identified Tyr320 in the hydrophobic pocket and Arg307, Asp309, Asn319 and Asp323 located around the pocket as critical for gelatin binding (Collier *et al.*, 1992). Two of these residues are located on a flexible loop comprised of residues 306–311 for which there is exceptionally poor density and high temperature factors. In the proMMP9 structure, the three FnII domains are oriented so that the respective hydrophobic pockets are pointed away from each other out toward solvent. These domains have minimal contact with the catalytic domain or with each other.

3.6. Comparison with MMP2 and other MMPs

The overall domain organization in proMMP9 is the same as that found in proMMP2. The structure of proMMP2 also included the hemopexin-like domain. In the proMMP2 structure, the large globular hemopexin-like domain has a small area of contact with the catalytic domain through an interaction with the loop between helices αB and αC at the C-terminus of the catalytic domain. It is uncertain as to whether the hemopexin-like domain of MMP9 would be in a similar relationship to the catalytic domain, since in proMMP9 the 20 kDa collagen-like domain is inserted between the hemopexin-like and catalytic domains.

The prodomains of MMP9 and MMP2 are identical in terms of placement of the cysteine-switch peptide in the active site. The N-terminus of the propeptide has a slightly different conformation in MMP2, but the conserved Phe31 that inserts into the hydrophobic pocket of the third FnII domain is conserved in MMP2 and plays an identical role in that molecule. The linker region between the propeptide and the catalytic domain (residues Gly105–Leu114) has a different conformation in the two molecules; however, flexibility of that

region is consistent with the higher temperature factors for those residues in each of the structures.

The FnII domains of MMP9 and MMP2 have very similar conformations, but placement of the FnII domains is not the same. With the MMP9 and MMP2 catalytic domains superimposed, the first and third FnII domains fall roughly in the same places, with the aromatic pockets oriented out toward solvent in each case. The second FnII domain of MMP2, however, has an extensive area of interaction with a loop of the catalytic domain, the loop between strand $\beta1$ and the first helix in the catalytic domain. The interaction of MMP2 with the catalytic domain occurs mostly through one MMP2 FnII domain extended loop, residues 306–311 (MMP9 numbering). In MMP9, however, the second FnII domain has rotated and twisted slightly away from the catalytic domain so that when the catalytic domains are superimposed as shown in Fig. 7, comparable residues of the second FnII domains of MMP9 and MMP2 are up to 21 Å apart. With this relative rotation, the second FnII domain in MMP9 does not interact at all with the catalytic domain. In the second FnII domain of MMP9, the contact loop, residues 306–311, appears to be quite flexible by virtue of the high temperature factors for the loop and its patchy electron density. In both MMP9 and MMP2, the second FnII domain is involved in crystal contacts. The domain has an extensive interface with a symmetry-related molecule in MMP2 and a small interaction with a symmetry mate in MMP9. Temperature factors are around the average for the protein for each of the MMP2 FnII domains, ~23 Å^2, while the overall average temperature factor for the second MMP9 FnII domain is significantly higher than the average for the full structure at 52 Å^2. This compares with average temperature factors of 37 Å^2 for proMMP9 and about 42 Å^2 for the other MMP9 FnII domains. Given (i) that the contact loop for the second FnII domain of MMP2 with the catalytic domain is flexible in MMP9, (ii) that the second FnII domain may be quite mobile in solution allowing an interaction of the MMP9 contact loop with the catalytic domain that would stabilize the structure of that loop and (iii) that these domains are involved in crystal contacts in both MMP2 and MMP9, there is no direct way to make use of the different positioning of the second FnII domain in designing inhibitors that would discriminate between MMP2 and MMP9.

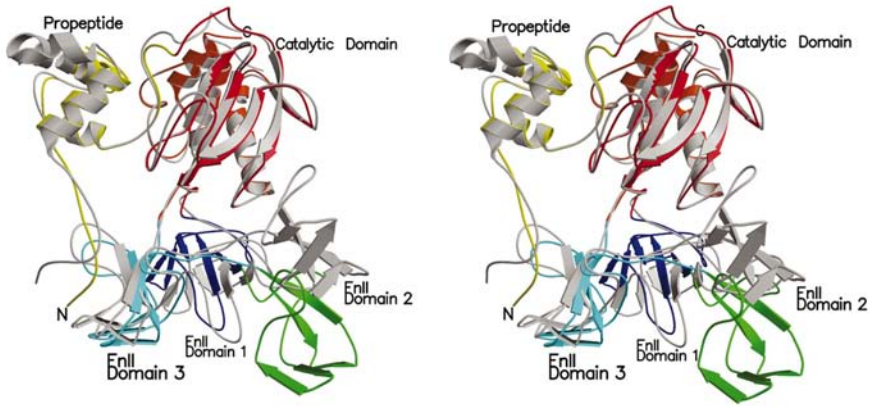

Figure 7
Superposition of the propeptide, catalytic and FnII domains of MMP9 and MMP2 (dark grey). The view shown has been rotated approximately 180° from the view shown in Fig. 2(*a*). The catalytic domains were superimposed with an r.m.s. deviation of approximately 1 Å. The MMP9 first and third FnII domains fall roughly in the same area with respect to the catalytic domain as the comparable domains in MMP2. The second MMP9 FnII domain, shown in green, is clustered with the other FnII domains, while the second MMP2 FnII domain interacts with the MMP2 catalytic domain.

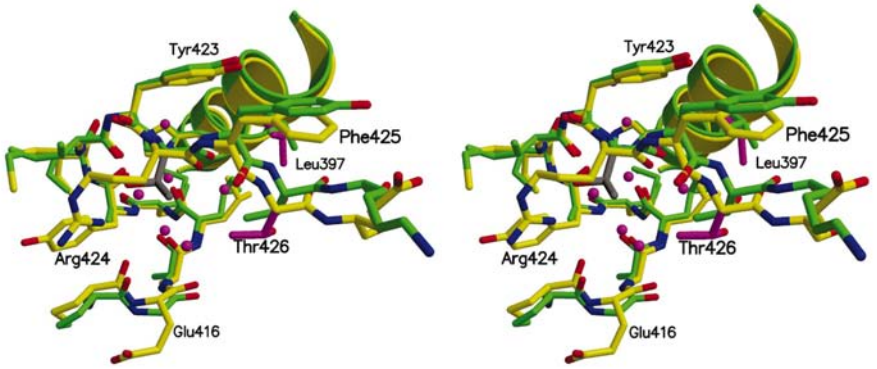

Figure 8
Superposition of the S1′ binding pockets of MMP9 and MMP2 (green). The proteins were superimposed using the C$^\alpha$ atoms of helix αB and residues 408–411. Helix αB is shown to the back of the figure. The S1′ pocket of MMP9 is filled with water molecules shown as small magenta balls. Residues that constrain the size of the pocket, Leu397 and Thr426, are shown in magenta for MMP9. The side chain of His401 forms another boundary to the S1′ pocket and can be seen extending from the helix. The figure is oriented such that the catalytic zinc would be behind the side chain of His401.

The ability to design an MMP9-specific inhibitor is a highly desired but challenging goal to achieve. The structure of the catalytic domain and of the active-site cleft is conserved in all MMP structures. In general, the shape and size of the S1′ binding pocket varies among structures of MMPs and contributes to the specificity of inhibitors. Residues that constrict the size of the S1′ pocket, residue 397 (arginine in MMP1) or residue 426 (arginine in MMP8) (Bode *et al.*, 1999; Li *et al.*, 1995; Stams *et al.*, 1994), are Leu397 and Thr426 in both MMP9 and MMP2, and leave the S1′ pocket open for possible interaction with larger P1′ constituents than may be accommodated in MMP1 or MMP8. In MMP3, although residues 397 and 426 are also small residues, comparison of the active site of MMP3 with that of MMP2 has revealed significant differences in the shape of the S1′ binding pockets of these MMPs (Dhanaraj *et al.*, 1999; Esser *et al.*, 1997).

In MMP9 and MMP2, many of the residues that make up the active-site cleft and the portion of the propeptide that sit in the active-site cleft are conserved and the side-chain conformations of these residues are also conserved. Fig. 8 shows a superposition of the S1′ binding pockets of MMP9 and MMP2. Differences in the active-site clefts between MMP9 and MMP2 are most noticeable in the stretch of residues that begins with residue 424 and continues into the specificity loop that curves around beyond residue 397 and serves as the back wall of the S1′ pocket. The only evident site for possible specificity discrimination between MMP9 and MMP2 centers around residue 424. The side chain of the preceding residue, the almost universally conserved Tyr423′, narrows the opening of the active-site cleft, potentially protecting a portion of bound inhibitor from solvent exposure. The identity of residue 424 varies among MMPs. In the active site of MMP2, Thr424 lines the S1′ pocket forming a boundary to the inhibitor-binding pocket. With the active sites of MMP9 and MMP2 superimposed by superimposing helix αB and the histidine ligands of the catalytic zinc, the backbone and side chain of Arg424 in MMP9 are slightly translated and angled away from the active site when compared with Thr424 of MMP2. This results in the C^{β} atom of residue Arg424 being almost 1 Å further from the center of the active-site cleft than the C^{β} atom of residue Thr424 in MMP2. The remainder of the Arg424 side chain points directly away from the S1′ pocket. Inhibitor-design studies will be needed to determine whether the conformation and position of Arg424 in MMP9 will allow the S1′ pocket to accommodate larger P1′ constituents than is possible in the S1′ pocket of MMP2. Thus, comparison of the active-site cleft of MMP9 with that of other MMPs suggests that design of inhibitors that discriminate between the gelatinases and other MMPs may be feasible and that an avenue for structure-based design exists to explore specificity between MMP2 and MMP9.

Data collection was carried out (in whole or in part) at the National Synchrotron Light Source, Brookhaven National Laboratory, which is supported by the US Department of Energy, Division of Materials Sciences and Division of Chemical Sciences under Contract No. DE-AC02-98CH10886. We are very grateful to Stephanie Van Horn and Marion Van Horn for DNA sequencing, and Joyce Mao for oligonucleotide synthesis.

References

Allan, J. A., Docherty, A. J., Barker, P. J., Huskisson, N. S., Reynolds, J. J. & Murphy, G. (1995). *Biochem. J.* **309**, 299–306.

Bacon, D. J. & Anderson, W. F. (1988). *J. Mol. Graph.* **6**, 219–220.

Banyai, L. & Patthy, L. (1991). *FEBS Lett.* **282**, 23–25.

Banyai, L, Tordai, H. & Patthy, L. (1994). *Biochem. J.* **298**, 403–407.

Bode, W., Fernandez-Catalan, C., Tschesche, H., Grams, F., Nagase, H. & Maskos, K. (1999). *Cell Mol. Life Sci.* **55**, 639–652.

Bode, W., Gomis-Ruth, F.-X. & Stocker, W. (1993). *FEBS Lett.* **331**, 134–140.

Brünger, A. T., Adams, P. D., Clore, G. M., DeLano, W. L., Gros, P., Grosse-Kunstleve, R. W., Jiang, J.-S., Kuszewski, J., Nilges, N., Pannu, N. S., Read, R. J., Rice, L. M., Simonson, T. & Warren, G. L. (1998). *Acta Cryst.* D**54**, 905–921.

Chen, L., Rydel, T. J., Gu, F., Dunaway, M., Pikul, S., Dunham, K. M. & Barnett, B. L. (1999). *J. Mol. Biol.* **293**, 545–557.

Collier, I. E., Krasnov, P. A., Strongin, A. Y., Birkedal-Hansen, H. & Goldberg, G. I. (1992). *J. Biol. Chem.* **267**, 6776–6781.

Collier, I. E., Wilhelm, S. M., Eisen, A. Z., Marmer, B. L., Grant, G. A., Seltzer, J. L., Kronberger, A., He, C. S., Bauer, E. A. & Goldberg, G. I. (1988). *J. Biol. Chem.* **263**, 6579–6587.

Coussens, L. M., Fingleton, B. & Matrisian, L. M. (2002). *Science*, **295**, 2387–2392.

Cowtan, K. (1994). *Jnt CCP4/ESF–EACBM Newsl. Protein Crystallogr.* **31**, 34–38.

Dhanaraj, V., Williams, M. G., Ye, Q.-Z., Molina, F., Johnson, L. L., Ortwine, D. F., Pavlovshy, A., Rubin, R., Skeean, R. W., White, A. D., Humblet, C., Hupe, D. J. & Blundell, T. L. (1999). *Croat. Chem. Acta*, **72**, 575–591.

Elliott, S. & Cawston, T. (2001). *Drugs Aging*, **18**, 87–99.

Esnouf, R. M. (1997). *J. Mol. Graph.* **15**, 132–134.

Esser, C. K. *et al.* (1997). *J. Med. Chem.* **40**, 1026–1040.

Galis, Z. S., Sukhova, G. K. & Libby, P. (1995). *FASEB J.* **9**, 974–980.

George, S. J. (2000). *Expert. Opin. Invest. Drugs*, **9**, 993–1007.

Jackson, C., Nguyen, M., Arkell, J. & Sambrook, P. (2001). *Inflamm. Res.* **50**, 183–186.

John, A. & Tuszynski, G. (2001). *Pathol. Oncol. Res.* **7**, 14–23.

Jones, T. A., Zou, J. Y., Cowan, S. W. & Kjeldgaard, M. (1991). *Acta Cryst.* A**47**, 110–119.

Kanayama, H. (2001). *J. Med. Invest.* **48**, 31–43.

Kraulis, P. J. (1991). *J. Appl. Cryst.* **24**, 946–950.

Kugler, A. (1999). *Anticancer Res.* **19**, 1589–1592.

Laskowski, R. A., MacArthur, M. W., Moss, D. S. & Thornton, J. M. (1993). *J. Appl. Cryst.* **26**, 283–291.

Li, J., Brick, P., O'Hare, M. C., Skarzynski, T., Lloyd, L. F., Curry, V. A., Clark, I. M., Bigg, H. F., Hazleman B. L. & Cawston, T. E. (1995). *Structure*, **3**, 541–549.

Li, Y. Y. & Feldman, A. M. (2001). *Drugs*, **61**, 1239–1252.

Lokeshwar, B. L. (1999). *Ann. NY Acad. Sci.* **878**, 271–289.

McCawley, L. J. & Matrisian, L. M. (2001). *Curr. Opin. Cell Biol.* **13**, 534–540.

Massova, I., Kotra, L. P., Fridman, R. & Mobashery, S. (1998). *FASEB J.* **12**, 1075–1095.

Merritt, E. A. M. & Murphy, M. E. P. (1994). *Acta Cryst.* D**50**, 869–873.

Morgunova, E., Tuuttila, A., Bergmann, U., Isupov, M., Lindqvist, Y., Schneider, G. & Tryggvason, K. (1999). *Science*, **284**, 1667–1670.

Morodomi, T., Ogata, Y., Sasaguri, Y., Morimatsu, M. & Nagase, H. (1992). *Biochem. J.* **285**, 603–611.

Murphy, G., Nguyen, Q., Cockett, M. I., Atkinson, S. J., Allan, J. A., Knight, C. G., Willenbrock, F. & Docherty, A. J. P. (1994). *J. Biol. Chem.* **269**, 5532–6636.

Okada, Y., Gonoji, Y., Naka, K., Tomita, K., Nakanishi, I., Iwata, K., Yamashita, K. & Hayakawa, T. (1992). *J. Biol. Chem.* **267**, 21712–21719.

Otwinowski, Z. & Minor, W. (1997). *Methods Enzymol.* **276**, 307–326.

Pickford, A. R., Potts, J. R., Bright, J. R., Phan, I. & Campbell, I. D. (1997). *Structure*, **5**, 359–370.

Sambrook, J., Fritsch, E. F. & Maniatis, T. (1989). *Molecular Cloning: A Laboratory Manual.* Cold Spring Harbor, NY, USA: Cold Spring Harbor Laboratory Press.

Schechter, I. & Berger, A. (1967). *Biochem. Biophys. Res. Commun.* **27**, 157–162.

Shaw, T., Nixon, J. S. & Bottomley, K. M. (2000). *Expert. Opin. Invest. Drugs*, **9**, 1469–1478.

Spinale, F. G., Coker, M. L., Bond, B. R. & Zellner, J. L. (2000). *Cardiovasc. Res.* **46**, 225–238.

Stams, T., Spurlino, J. C., Smith, D. L., Wahl, R. C., Ho, T. F., Qoronfleh, M. W., Banks, T. M. & Rubin, B. (1994). *Nature Struct. Biol.* **1**, 119–123.

Stocker, W. & Bode, W. (1995). *Curr. Opin. Struct. Biol.* **5**, 383–390.
Stocker, W., Grams, F., Baumann, U., Reinemer, P., Gomis-Ruth, F.-X., McDay, D. B. & Bode, W. (1995). *Protein Sci.* **4**, 823–840.
Terwilliger, T. C. & Berendzen, J. (1999). *Acta Cryst.* D**55**, 849–861.
Triebel, S., Blaser, J., Reinke, H., Knauper, V. & Tschesche, H. (1992). *FEBS Lett.* **298**, 280–284.
Van Wart, H. E. & Birkedal-Hansen, H. (1990). *Proc. Natl Acad. Sci. USA*, **87**, 5578–5582.
Wilhelm, S. M., Collier, I. E., Marmer, B. L., Eisen, A. Z., Grant, G. A. & Goldberg, G. I. (1989). *J. Biol. Chem.* **264**, 17213–17221.
Woessner, J. F. Jr (1991). *FASEB J.* **5**, 2145–2155.
Wojtowicz-Praga, S. M., Dickson, R. B. & Hawkins, M. J. (1997). *Invest. New Drugs*, **15**, 61–75.
Yao, J., Xiong, S., Klos, K., Nguyen, N., Grijalva, R., Li, P. & Yu, D. (2001). *Oncogene*, **20**, 8066–8074.
Zucker, S., Hymowitz, M., Conner, C., Zarrabi, H. M., Hurewitz, A. N., Matrisian, L., Boyd, D., Nicolson, G. & Montana, S. (1999). *Ann. NY Acad. Sci.* **878**, 212–227.